acta physica slovaca vol. 51 No. 4, 261 – 270 **August 2001**

HOLOGRAPHIC INTERFEROMETRY USING A DIGITAL PHOTO-CAMERA

H. Sekanina[1], **S. Hledík**[2]
Department of Physics, Faculty of Philosophy and Science, Silesian University, Bezručovo nám. 13, 746 01 Opava, Czech Republic

Received 9 July 2001, in final form 17 July 2001, accepted 18 July 2001

The possibilities of running digital holographic interferometry using commonly available compact digital zoom photo-cameras are studied. The recently developed holographic setup, suitable especially for digital photo-cameras equipped with an undetachable object lens, is used. The method described enables a simple and straightforward way of both recording and reconstructing of a digital holographic interferogram. The feasibility of the new method is verified by digital reconstruction of the interferograms acquired, using a numerical code based on the fast Fourier transform. Experimental results obtained are presented and discussed.

PACS: 42.25.-p, 42.30.-d, 42.40.-i

1 Introduction

Classical ray interferometry enables the measurement and comparisons of length variations along a fixed direction. On the other hand, in holographic interferometry we compare the whole surfaces of the objects under consideration and the displacement of individual points of the whole surface can be determined. Using holographic interferometry we compare (with accuracy corresponding to approximately one tenth of the wavelength used) two partly coherent waves, at least one of which being obtained by reconstruction of the corresponding hologram. Since the waves compared by the holographic interferometry are coherent and situated at the same region of the space, they interfere letting an interference pattern (holographic interferogram) arise. The knowledge of the interference pattern distribution enables us to determine the displacement vector of each point at the object's surface.

Nowadays the optical holographic interferometry can be divided into two main groups: the classical holographic interferometry and the digital holographic interferometry. The typical features of the classical holographic interferometry are the following:

- The holograms are recorded on a medium with a high resolution of thousands interference line pairs per millimetre (1000–5000 lines/mm). A good example of a reliable medium with such a resolution is, even today, a photographic plate or a film.

[1]E-mail address: Hynek.Sekanina@fpf.slu.cz.
[2]E-mail address: Stanislav.Hledik@fpf.slu.cz.

- The reconstruction of the interferograms obtained have to be carried out physically by means of light in an optical laboratory, which forms the holographic interferogram existing in reality. The holographic interferogram must be evaluated by means of other techniques. The surface of localisation of the interference pattern has to be established as a part of the evaluation. Moreover, it is possible to compare holographically reconstructed wave, and the wave reflected by the real object (holographic interferometry in real time).

The typical features of the digital holographic interferometry are the following:

- The hologram recording is carried out on modern digital media, which still means media having a relatively low resolution. The main feature of these media is that they change some of their electric characteristic by the incidence of the light wave. The typical examples are the CCD or CMOS chips. CCD chips consist of a certain number of points—pixels. Each pixel allows either monochromatic (a certain number of grey levels) or colour recording (again with the given bit depth in each of the three basic colours). The number of pixels and the size of each of them are the principal characteristics of the CCD chips, the typical values commonly available at present are [1, 2]: pixel size $\Delta x = 5$–11 μm, color depth 10–14 bits for each of the three basic colors (optionally 10–14 bits for grey levels in the case of monochromatic CCD chips), the number of pixels about 500–2000×500–1500 and the diagonal size of the whole CCD chip about $1/2$–$2/3$ inch. The pixel size determines the resolution of the whole CCD chip. Even with the state-of-the-art technology, the chip resolution is low (approximately 100 lines/mm) when comparing, e.g., both with available photoplates and from the aspect of holographic interferometry demands (in the region of the visible light).

- The reconstruction is not carried out physically in a laboratory but by means of numerical methods using a computer. This is because the holograms recorded on CCD cannot be reconstructed by light physically. Therefore, the holographic interferometry in real time is excluded, and both compared waves must be obtained holographically. However, the computer reconstruction of digital holograms has remarkable advantage: the simulation of real reconstruction is possible, but not necessary. Using a computer code, we can directly calculate the phase map [3] that enables direct determination of the displacement vector for each surface point (without localisation of interference pattern surface).

In the optimal way, the digital holographic interferometry can be run with special CCD arrays that can be directly inserted into the interference field. The main purpose of this article is to demonstrate that the holographic interferometry can be run successfully also without specialized equipment using currently available digital photo-cameras with undetachable object lens (usually called compact photo-cameras).

2 Method

The hologram reconstruction is in principle diffraction of the reconstructing wave at a hologram pattern. Given the hologram—a plane transparency with a real amplitude transmittance $t \in \langle 0, 1 \rangle$ proportional to the intensity of the sum of the reference wave U_r and the object wave U_o,

$$t \propto |U_\mathrm{r} + U_\mathrm{o}|^2 = I_\mathrm{r} + I_\mathrm{o} + U_\mathrm{r}^* U_\mathrm{o} + U_\mathrm{r} U_\mathrm{o}^*, \tag{1}$$

we can reconstruct the object wave by illuminating the hologram with the reference wave again. The result is a wave with complex amplitude

$$U = tU_{\mathrm{r}} \propto U_{\mathrm{r}}I_{\mathrm{r}} + U_{\mathrm{r}}I_{\mathrm{o}} + I_{\mathrm{r}}U_{\mathrm{o}} + U_{\mathrm{r}}^2U_{\mathrm{o}}^* \tag{2}$$

in the hologram plane. The third term on the right-hand side is the object wave multiplied by the intensity I_{r} of the reference wave. If I_{r} is uniform across the transparency, this term constitutes the desired reconstructed wave. The fourth term is a conjugated version of the object wave modulated by U_{r}^2. The first two terms represent the reference wave, modulated by the sum of the intensities of the two waves.

In the following we shall identify the hologram plane with the plane $z = 0$, i.e., with the xy plane. The amplitude transmittance of the hologram then depends on the two coordinates only, $t \equiv t(x, y)$. Further, we shall select the reference wave to be a uniform monochromatic plane wave propagating along the z axis. The reference wave will be termed 'reconstructing' henceforth.

2.1 The Fresnel approximation

Now, we shall focus on how the light field propagates along the positive direction of the z axis, i.e., how the image is reconstructed by diffraction of the reconstructing wave at the hologram microstructure.

The Huygens–Fresnel principle [4] states that each point on a wavefront generates a spherical wave. The envelope of these secondary waves constitutes a new wavefront, and their superposition constitutes the wave in another plane, say, $z = d$.

Let us consider a point with coordinates (ξ, η, d) lying at the $z = d$ plane. According to the Huygens–Fresnel principle, the light complex disturbance $\mathrm{d}g(\xi, \eta)$ caused by the spherical wave originated in an infinitesimal portion of area $\mathrm{d}x\mathrm{d}y$ at a point $(x, y, 0)$ in the transparency plane is proportional to the amplitude transmittance $t(x, y)$, the area of the spot $\mathrm{d}x\mathrm{d}y$, the phase factor (the time dependence is omitted), and inversely proportional to the distance between the two points considered:

$$\mathrm{d}g(\xi, \eta) \propto t(x, y)\frac{\exp(-\mathrm{i}\vec{k}\cdot\vec{R})}{R}\,\mathrm{d}x\mathrm{d}y, \tag{3}$$

where the vector $\vec{R} \equiv (\xi - x, \eta - y, d)$ is pointing from the center of the spherical wave to the point in which the disturbance is to be calculated, $R \equiv |\vec{R}|$ is the modulus of $\vec{R}$, and $\vec{k} = (2\pi/\lambda)\vec{R}/R$ is the propagation vector. With this in mind, it is easy to show that the scalar product in the argument of the exponential function in Eq. (3) can be expressed as

$$\vec{k}\cdot\vec{R} = 2\pi\frac{d}{\lambda}\sqrt{1 + \frac{(\xi - x)^2 + (\eta - y)^2}{d^2}} = 2\pi\frac{d}{\lambda}\sqrt{1 + \mathcal{S}_{\vec{\rho}}}, \tag{4}$$

where we introduced

$$\mathcal{S}_{\vec{\rho}} \equiv \frac{\rho_x^2 + \rho_y^2}{d^2} \tag{5}$$

and the projection of the vector $\vec{R}$ onto the transparency plane

$$\vec{\rho} \equiv (\xi - x, \eta - y, 0). \tag{6}$$

If the values of the $\mathcal{S}_{\vec{\rho}}$ are negligible in comparison with unity for all values of $\vec{\rho}$ considered, $\max\{|\xi - x|, |\eta - y|\} \ll d$, we can use the power expansion

$$\sqrt{1 + \mathcal{S}_{\vec{\rho}}} = 1 + \frac{1}{2}\mathcal{S}_{\vec{\rho}} + \mathcal{O}\left(\mathcal{S}_{\vec{\rho}}^2\right). \tag{7}$$

While the exponential is very sensitive to the change of $\vec{R}$, the R^{-1}-factor in (3) can be replaced with a constant value of d without loss of accuracy. Hence Eq. (3) can be rewritten as

$$\mathrm{d}g(\xi,\eta) \propto \frac{1}{d}\, t(x,y)\, \exp\left\{-\mathrm{i}\pi\frac{d}{\lambda}\left[\mathcal{S}_{\vec{\rho}} + \mathcal{O}(\mathcal{S}_{\vec{\rho}}^2)\right]\right\} \mathrm{d}x\mathrm{d}y, \tag{8}$$

where we omitted the constant factor $\exp(-\mathrm{i}2\pi d/\lambda)$. The total disturbance in any point (ξ, η) in the output plane $z = d$ can be determined by integrating (8) over whole the xy plane:

$$g(\xi,\eta) = h_0 \iint_{-\infty}^{+\infty} t(x,y)\, \exp\left\{-\mathrm{i}\pi\frac{d}{\lambda}\left[\mathcal{S}_{\vec{\rho}} + \mathcal{O}(\mathcal{S}_{\vec{\rho}}^2)\right]\right\} \mathrm{d}x\mathrm{d}y. \tag{9}$$

The constant factor h_0 includes, in addition to $1/d$ and the constant complex unit $\exp(-\mathrm{i}2\pi d/\lambda)$, the amplitude of the reconstructing wave. The definition of the impulse-response function [5]

$$h(x,y) \equiv h_0\, \exp\left\{-\mathrm{i}\pi\frac{d}{\lambda}\left[\mathcal{S}_{\vec{r}} + \mathcal{O}(\mathcal{S}_{\vec{r}}^2)\right]\right\} \tag{10}$$

with $\vec{r} \equiv (x, y, 0)$ enables to interpret Eq. (9) in terms of theory of linear systems as the two-dimensional convolution of the amplitude transmittance and the impulse-response function (10):

$$g(\xi,\eta) = \iint_{-\infty}^{+\infty} t(x,y) h(\xi - x, \eta - y)\, \mathrm{d}x\mathrm{d}y. \tag{11}$$

If we restrict ourselves to the $\mathcal{S}^1$-term only, the impulse-response function (10) will simplify to Fresnel approximation impulse-response function

$$h(x,y) \equiv h_0\, \exp\left(-\mathrm{i}\pi\frac{x^2 + y^2}{\lambda d}\right) \tag{12}$$

which converts the formula (9) into a simpler form

$$g(\xi,\eta) = h_0 \iint_{-\infty}^{+\infty} t(x,y)\, \exp\left[-\mathrm{i}\pi\frac{(\xi - x)^2 + (\eta - y)^2}{\lambda d}\right] \mathrm{d}x\mathrm{d}y, \tag{13}$$

where spherical waves are approximated by paraboloidal waves. The term impulse-response function arises from the property that such function represents the response to an impulse input, namely the Dirac δ-function. Indeed, substituting $t(x, y) = \delta(x, y)$ into Eq. (10) yields $g(\xi, \eta) = h(\xi, \eta)$.

In summary, the space-domain approach described above is based on a treatment in which the input wave is expanded in terms of spherical elementary waves (or in terms of paraboloidal elementary waves in Fresnel approximation).

Now it remains to clarify the condition of validity of the Fresnel approximation. The Fresnel approximation holds if the 1. post-Fresnelian $\mathcal{S}^2$-term in the impulse-response function (10) is

much smaller than π for all $\vec{\rho}$, i.e., $\pi d\mathcal{S}^2/(4\lambda) \ll \pi$. Using the definition of $\mathcal{S}$ (5), we can find this to be equivalent to $\rho^4 \ll 4\lambda d^3$. Denoting a the largest radial distance in the output plane $\xi\eta$, it is clear that $\rho^2 \leq a^2$, so that the condition of validity of the Fresnel approximation may be written in the form

$$a^4 \ll 4\lambda d^3 \tag{14}$$

or equivalently

$$\frac{1}{4} N_{\mathrm{F}} \theta_{\max}^2 \ll 1, \tag{15}$$

where

$$N_{\mathrm{F}} \equiv \frac{a^2}{\lambda d} \tag{16}$$

is the Fresnel number and

$$\theta_{\max} \approx \frac{a}{d} \tag{17}$$

is the largest angle corresponding to a. The integral (13) can be rewritten in the form

$$g(\xi,\eta) = h_0 \, \exp\left[-\mathrm{i}\frac{\pi}{\lambda d}(\xi^2+\eta^2)\right] \iint_{-\infty}^{\infty} \tilde{t}(x,y) \, \exp\left[\mathrm{i}\frac{2\pi}{\lambda d}(\xi x + \eta y)\right] \, \mathrm{d}x\mathrm{d}y, \tag{18}$$

where we denoted

$$\tilde{t}(x,y) \equiv t(x,y) \, \exp\left[-\mathrm{i}\frac{\pi}{\lambda d}(x^2+y^2)\right]. \tag{19}$$

Hence, when restricted to Fresnel approximation, the output function can be conveniently calculated via fast Fourier transform techniques.

Having calculated the complex amplitude $g(x,y)$ in the output plane, we can immediately determine the intensity by taking the modulus and squaring

$$I(x,y) = |g(x,y)|^2 = [\mathrm{Re}\, g(x,y)]^2 + [\mathrm{Im}\, g(x,y)]^2. \tag{20}$$

The phase can be calculated as

$$\Phi(x,y) = \arctan \frac{\mathrm{Im}\, g(x,y)}{\mathrm{Re}\, g(x,y)}, \tag{21}$$

where the inverse tangent used in (21) must be capable to recognize the quadrant to ensure $\Phi \in \langle -\pi, \pi \rangle$.

2.2 Numerical treatment

The function $g(\xi,\eta)$ can be digitized if the hologram transmission function $t(x,y)$ is sampled on a rectangular raster of $N_x \times N_y$ matrix points, with steps Δx and Δy along the coordinates. Then the discrete representation of Eq. (18) is given by the following formula [3]:

$$\begin{aligned} g(m,n) = \; & \exp\left[-\mathrm{i}\pi\lambda d\left(\frac{m^2}{N_x^2\Delta x^2}+\frac{n^2}{N_y^2\Delta y^2}\right)\right] \\ & \times\left\{\sum_{k=0}^{N_x-1}\sum_{l=0}^{N_y-1} t(k,l)\,\exp\left[-\mathrm{i}\frac{\pi}{\lambda d}(k^2\Delta x^2+l^2\Delta y^2)\right]\right. \\ & \left.\times\;\exp\left[\mathrm{i}2\pi\left(\frac{km}{N_x}+\frac{ln}{N_y}\right)\right]\right\}. \end{aligned} \tag{22}$$

From the numerical point of view, Eq. (22) can be calculated efficiently using the fast Fourier transform (FFT) [6]. The function to be Fourier transformed is the product of $t(k,l)$ with the first exponential factor in the sum. In the calculation of the transformation, the standard 'radix 2 Cooley–Tukey' (see, e.g., [6]) has been applied. The factor before the sum is a complex unit and can be omitted when calculating the intensity. The code developed is capable

1. to read an input file (recorded hologram), using them to calculate intensity, phase and complex amplitude according to Eqs (18), (20), (21) and (22);
2. to perform per-pixel subtraction or addition of two input files containing complex amplitudes;
3. to perform per-pixel subtraction of two input files containing phase, using them to produce the modulus of the difference of phases modulo 2π, i.e.,

$$\Delta\Phi \equiv \begin{cases} \Phi_1-\Phi_2 & \text{if} \quad \Phi_1 \le \Phi_2, \\ \Phi_1-\Phi_2+2\pi & \text{if} \quad \Phi_1 < \Phi_2. \end{cases} \tag{23}$$

2.3 The possibilities of numerical reconstruction

The computer reconstruction runs similarly as the physical one—the recorded hologram is 'illuminated' by the wave corresponding to the recording reference wave, thereby getting the corresponding object images.

However, in order to obtain interferometric results we don't have to simulate the real laboratory reconstruction only.

The real reconstruction simulation possibilities:

1. At first we perform addition of amplitude transmittances of two chosen holograms, then the sum can be numerically reconstructed. Of course we get object images (corresponding to the classical holographic interferograms) overlaid with interference pattern which characterizes object changes between hologram exposures. This process is simulation of two exposure holographic interferometry. This approach involves one hologram reconstruction; the interferogram obtained must be interpreted by additional methods.

2. Because the correspondence $t(k,l)$ and $g(m,n)$ in (22) is linear, we can consider a version of the previous procedure in which we reconstruct each hologram separately and then add the reconstructed complex amplitudes.

The possibilities over real simulation are as follows:

3. In compliance with [7], it is also possible to subtract the amplitude transmittances of two holograms, to reconstruct the difference obtained. Generally it is claimed [7] that subtraction gives better results in the contrast of the interference pattern. However, our results do not confirm this conclusion.

4. We use the method from [3] which enables not only the direct calculation of the intensity, i.e., the intensity acquired of the usual holographic interferogram, but also the direct phase computation for each hologram. The phase difference modulo 2π defined by Eq. (23) calculated for each pixel—the phase map—is than the direct visualization of the corresponding changes of the examined object surface. We spread the treatment in [3] to the arrangement using lenses during the hologram record on the photo-camera CCD chip.

Further, the digital filtering can be applied to remove the reconstructing wave modulated by the sum of the intensities of the reconstructing and object wave, i.e., the first two terms in Eq. (2). The digital high-pass filter and its enhanced version (bandpass filter) were used.

3 Hologram recording

High-quality CCD chips in present photo-cameras consist of several million pixels. The experimental investigations were carried out with Olympus CA3000 Zoom photo-camera, which is at disposal in our optical laboratory. The CCD array of the camera used consists of 2048 pixels in horizontal direction and 1536 pixels in vertical direction, the pixel size is $\Delta x = 5.51\ \mu$m in both directions.

As mentioned above, digital real time holographic interferometry is not realisable, only the double-exposure method or the sandwich holography can be used. Holographic interferometry termed sandwich holography [7] is a very useful modification of the double-exposure method because it eliminates some serious disadvantages of the double-exposure method. Just sandwich holography is used in this article. As most digital photo-cameras (including Olympus CA3000 Zoom photo-camera) are equipped with the undetachable object lens, we used for the hologram recording arrangement attested in the recent article [8]. The arrangement is a version of the classical 'off-axis' holography characterised by a nonzero holographic angle.

The mentioned arrangement considers the affect of the photo-camera object lens on the recorded interferometric field. If we use the camera's zoom (the transverse optical magnification $Z = 3$ in our case) and the camera's object lens is focused on its minimal distance (20 cm in our case), the passage of the light through the object lens increases the interference field frequencies about $7\times$. Considering the used photo-camera CCD chip parametres and applying the sample theorem [6] we get the maximal recordable spatial frequency $f_{\max} = (2 \times 5.51\ \mu\mathrm{m})^{-1}$. From the well known formula

$$f = \frac{2}{\lambda} \sin \frac{\vartheta}{2}\,, \tag{24}$$

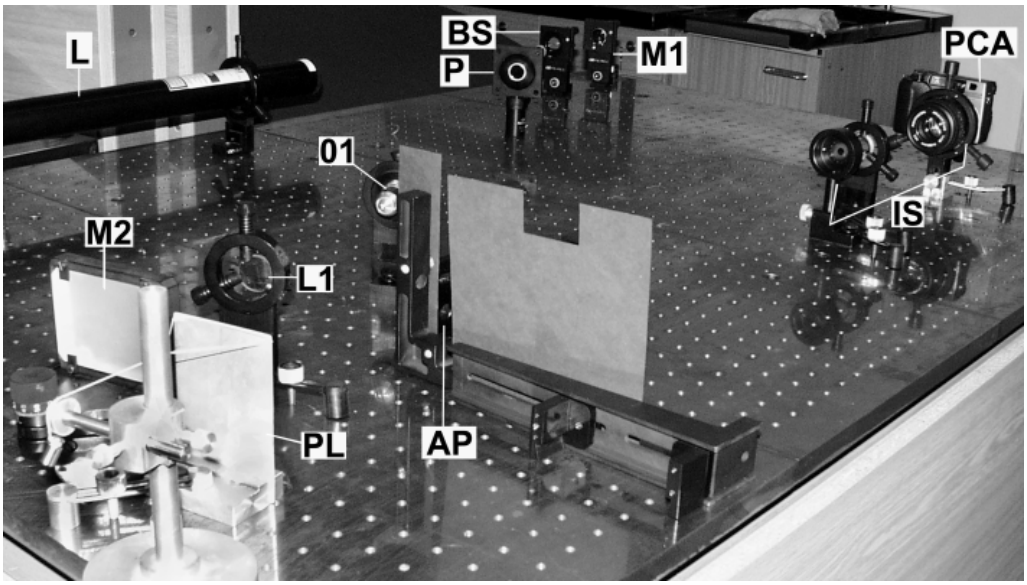

Fig.1. A photograph of the holographic table arrangement used: *L*, laser; *BS*, beamsplitter; *M1*, *M2*, mirrors; *P*, polarizer; *O1*, objective; *L1*, lens; *IS*, imaging system described in [8]; *PL*, aluminium plate; *AP*, aperture; *PCA*, digital photo-camera.

which determines the interference field spatial frequency f of the two plane monochromatic waves (with the wavelenght λ, $\lambda = 632.8\,\mathrm{nm}$ in our case) containing angle ϑ, we obtain that the angle ϑ must fulfil the condition $\vartheta \leq 5.31^\circ$.

We can conclude that the relatively low CCD chip resolution limits the holographic angle ϑ, that may be used for hologram recording, on the mentioned value of several degrees. It results — see Fig. 1 — the objects of the maximal diameter about 3 cm (plate *PL*) situated at a distance of 73 cm from the imaging system *IS* can be holographed.

The main advantage of the used 'off-axis' holography over the 'in-line' holography is that even with the holographic angle of single degrees, the reconstructed images are spatially separated. Using the sandwich holography, each of the approaches described in the subsection 2.3 enables comparison of arbitrary two surface states of the object (i.e., each i state with each j state, where i, j corresponds always to one of n recorded holograms). Thus using the sandwich holography, we record always one hologram on one photograph. The recorded hologram data are loaded into the computer and stored (in the TIFF format) on the hard disk.

4 Experimental results

The possibilities of holographic interferometry using the digital photo-camera were tested using the apparatus Olympus camera CA3000 Zoom which parameters can be found for instance on URL [9] and its applicability in holography was discussed in [8]. For the hologram recording we used the arrangement from [8], the photograph illustrated the setup realization on the holographic table is in Fig. 1. The light from the linear polarized He-Ne laser *L* ($\lambda = 632.8\,\mathrm{nm}$) with an

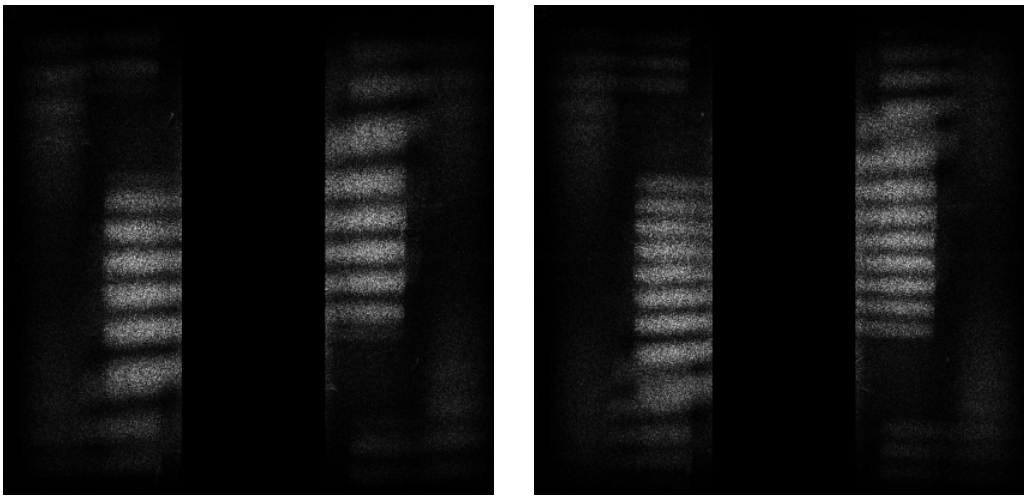

(a) (b)

Fig. 2. Two interferograms chosen as the demonstration of the digital hologram interferometry using the digital photo-camera. (a) The interferogram corresponding to the change of the weights from 7 g to 2 g. (b) The interferogram corresponding to the change of the weights from 2 g on 0 g. Both the primary (the left parts of the images) and the secondary (the right parts of the images) interference pattern can be seen. Both interferograms were obtained by the method described in the subsection 2.3 as possibility 1. The central maximum is completely suppressed using high-pass filtering.

energy output of $P = 50$ mW is divided by a beam-splitter BS into an object wave and reference wave at the ratio of intensities 95% to 5%. The object wave is expanded by a microscopic object lens *O1* (magnification $M = 40$) and incidents on the tested object *PL*—the aluminium plate (dimensions 8×4 cm) placed in a stable holder. The whole tested plate, which could be deformed by hanging of weight by means of thread, was illuminated.

The reference wave is reduced by the polarizer *P* and after its passage through the lens *L1* incidents on a mirror *M2* placed beside the illuminated plate. The object and the reference wave interfere (the used aperture *AP* only reduces the dimensions of the object wave in the horizontal direction on about 2 cm, so that we record holograms of object of the size about 8×2 cm which should respond to the maximum of today digital holography) and after its passage through the optical imaging system *IS* described in [8], the interference field is photographed by the Olympus camera CA3000 Zoom (*PCA*) by which we get the hologram. Taking snaps of interference pattern we used the camera's control comfort including its remote control, exposure and focusing automatics. The value of the deformation power was changed among each two exposures (exposure time about $1/5$ s).

As we used the sandwich holography one hologram was recorded on one photograph, the presented results correspond to weights 7 g, 2 g and 0 g. The hologram files (2048×1536 pixels) were loaded into the computer and stored. The TIFF format was converted to PPM format, from each hologram was done the cutout of the size 1024×1024 pixels. Numerical reconstructions named in the section 2.3 ware performed using the prepared computer code.

So, in the Fig. 2a we can see the holographic interferogram corresponding to the change of

the weights from 7 g to 2 g. In the Fig. 2b is depicted the interferogram corresponding to the change of the weights from 2 g to 0 g. Both the primary (always the left part of image) and the secondary (the right part of images) holographic images can be seen. Both interferograms were obtained by the method described in the subsection 2.3 as possibility 1. The spurious central maximum is always completely suppressed using high-pass filtering.

5 Conclusions

The possibilities of the realisation of the digital holographic interferometry using the digital photo-camera have been discussed and tested, the experimental results have been presented. Various approaches to the numerical reconstruction are listed. The efficient computer code performing the digital hologram reconstruction has been developed.

As the results obtained are distinct and can be reproduced easily, we have demonstrated that the digital holographic interferometry can be run without the specialized equipment. The problems concerning holographic interferometry using a digital photo-camera are very interesting and the method has promising perspectives. Our another work may be dedicated to the optimalization of the digital reconstruction.

We can conclude it seems to be useful trying to find proper feasibility of using the described variant of holographic interferometry in praxis—generally in the surface inspection but also, for instance, in the artwork diagnostics. We hope that with the development of the technology, a constant expansion of the use of the digital holographic interferometry will occur.

Acknowledgements The authors thank prof. Z. Stuchlík for his support and valuable discussions.

References

[1] `http://www.baslerweb.com/en/products/`

[2] `http://www.photobit.com/Products/Product_Matrix/product_matrix.htm`

[3] U. Schnars: *J. Opt. Soc. Am. A* **11** (1994) 2011

[4] M. Born, E. Wolf: *Principles of Optics*, 6th edition, Pergamon Press, Oxford 1980

[5] B. E. A. Saleh, M. C. Teich: *Fundamentals of Photonics*, John Wiley & Sons, New York 1991

[6] W. H. Press, S. A. Teukolsky, W. T. Vetterling, B. P. Flannery, *Numerical Recipes in C (The Art of Scientific Computing)*, 2nd edition, Cambridge Univ. Press, Cambridge 1992

[7] D. Paoletti, G. S. Spagnolo: in *Progress in Optics* (Ed. E. Wolf). North Holland, Amsterdam 1996, p. 197

[8] H. Sekanina, J. Pospíšil: *Digital holography using a digital photo-camera*, submitted to Journal of Modern Optics

[9] `http://cf.olympus-europa.com/consumer/digimg/intro.cfm?id=C-3000ZOOM`